



Article

Deep Learning Vision System for Quadruped Robot Gait Pattern Regulation

Christyan Cruz Ulloa , Lourdes Sánchez, Jaime Del Cerro and Antonio Barrientos *

Centro de Automática y Robótica (CSIC-UPM), Universidad Politécnica de Madrid—Consejo Superior de Investigaciones Científicas, 28006 Madrid, Spain; christyan.cruz.ulloa@upm.es (C.C.U.); lourdes.sanchezl@alumnos.upm.es (L.S.); j.cerro@upm.es (J.D.C.)

* Correspondence: antonio.barrientos@upm.es

Abstract: Robots with bio-inspired locomotion systems, such as quadruped robots, have recently attracted significant scientific interest, especially those designed to tackle missions in unstructured terrains, such as search-and-rescue robotics. On the other hand, artificial intelligence systems have allowed for the improvement and adaptation of the locomotion capabilities of these robots based on specific terrains, imitating the natural behavior of quadruped animals. The main contribution of this work is a method to adjust adaptive gait patterns to overcome unstructured terrains using the ARTU-R (A1 Rescue Task UPM Robot) quadruped robot based on a central pattern generator (CPG), and the automatic identification of terrain and characterization of its obstacles (number, size, position and superability analysis) through convolutional neural networks for pattern regulation. To develop this method, a study of dog gait patterns was carried out, with validation and adjustment through simulation on the robot model in ROS-Gazebo and subsequent transfer to the real robot. Outdoor tests were carried out to evaluate and validate the efficiency of the proposed method in terms of its percentage of success in overcoming stretches of unstructured terrains, as well as the kinematic and dynamic variables of the robot. The main results show that the proposed method has an efficiency of over 93% for terrain characterization (identification of terrain, segmentation and obstacle characterization) and over 91% success in overcoming unstructured terrains. This work was also compared against main developments in state-of-the-art and benchmark models.

Keywords: biologically inspired robotics; quadruped robots; convolutional neural networks; robotics vision; transfer learning



Citation: Cruz Ulloa, C.; Sánchez, L.; Del Cerro, J.; Barrientos, A. Deep Learning Vision System for Quadruped Robot Gait Pattern Regulation. *Biomimetics* **2023**, *8*, 289. <https://doi.org/10.3390/biomimetics8030289>

Academic Editor: James Whiting

Received: 3 April 2023

Revised: 12 June 2023

Accepted: 20 June 2023

Published: 3 July 2023



Copyright: © 2023 by the authors. Licensee MDPI, Basel, Switzerland. This article is an open access article distributed under the terms and conditions of the Creative Commons Attribution (CC BY) license (<https://creativecommons.org/licenses/by/4.0/>).

1. Introduction

The research and development of bio-inspired quadruped robots have evolved in recent decades, resulting in robots with a great capacity for mimicry and locomotion modes inspired by animal behavior in nature. In these developments, intelligence systems should be highlighted. Biomimicry allows us to solve complex problems, such as moving through complex environments, a topic currently of interest at the research level [1].

Among the main challenges and limitations of this type of robot is its movement through unstructured terrain, with the presence of debris. In this way, terrestrial animals such as horses [2] and snakes [3] have inspired several robotic developments, allowing them to move with great agility in nature.

On the other hand, search-and-rescue robotics arise from the need to assist rescue brigades in interventions at post-disaster events, seeking to protect lives and help detect victims in the environment [4,5]. Historically, bio-inspired robots, such as those of the caterpillar type, have been used in this type of intervention, including: the United States (Twin Towers, 2001) [4,6], Japan (Fukushima, 2011) [7], Italy (Amatrice, 2016) [8] and Mexico (2017) [9].

The rise of quadruped robots has made it possible to explore new alternatives for exploration and displacement in rustic terrain, given their great agility, fast response times,

omnidirectional movement, and ability to perform even in terrains where robots with conventional locomotion systems (wheels or caterpillars) are not able to [10].

Quadruped robots currently use LiDAR-based systems to locate and identify the terrain [11], which faces disadvantages in accurately characterizing stable zones and surmountable obstacles, or they generalize the terrain using specific contact sensors for the characterization of materials [12,13]. However, real scenarios, by nature, are constantly changing, unstructured and unstable, which represents a challenge within state-of-the-art robotic systems in adjusting gait patterns. This will be addressed in the first approach of this study. On the other hand, there have been methods developed to generically identify the type of terrain [14–16], but the problem of characterizing its elements is not focused, and the obstacles that represent a challenge for mobility on these surfaces are not structured.

The main contribution of this work is overcoming the challenges of unstructured terrain using the ARTU-R quadruped robot (A1 Rescue Task UPM Robot), automatically adjusting the kinematic and dynamic parameters of its gait patterns based on the identification of the terrain using a central pattern generator and characterization of the terrain obstacles using neural networks for gait pattern regulation.

To this end, a simulation phase was started in environments by ROS-GAZEBO to validate a virtual model of the robot, using the gait patterns studied in dogs to determine the relevant parameters of the walk, which would later be adjusted based on the information output from the neural network. The adjustments of the kinematic and dynamic parameters of the robot's gait patterns were made based on the automatic analysis of the terrain type (gravel, earth or grass) and the type of obstacles in it.

This automatic recognition and semantic segmentation of the environment was carried out by training a convolutional neural network (YOLOv8) using a dataset of more than 1700 images. Tests were carried out in real environments to validate the proposed method, with successful results in overcoming unstructured terrain with the robot.

This paper is structured as follows: Section 2 shows the most relevant works on terrain identification and characterization. Section 3 details the materials and methods used. Section 4 describes the experiments and results. Finally, the main findings are presented in Section 5.

2. Related Work

2.1. Automatic Terrain Identification Robotic Systems

The identification and characterization of environments is a widely studied problem in robotics perception to determine the specific characteristics of the environment in order to define advance and displacement strategies. The main methods used for this task are LiDAR-type sensors, RGB-D cameras and sensors for material characterization [17]. In this way, two subsections can be established for identifying terrain: sensors that require contact with the soil material and visual-type sensors.

2.1.1. Identification Based on Contact Sensors

Common terrain identification methods use specific sensors built into the robot's legs. These sensors are distributed to identify different types of materials [12,13,18,19] and allow locomotion parameters to be adjusted for the robots depending on the terrain. For their part, other robots with hexapod legs use force/torque sensors and Bayesian-type classifiers to determine terrain type [20].

Others base their functionality on vibration systems combined with linear discriminant analysis to characterize the terrain, mainly types similar to the Martian rover [21–23].

Contact-based systems for land identification show promising results when there is complete contact, but they face a series of problems when there is no complete contact due to debris or there is a generalization of the entire terrain based on local measurements. Another disadvantage is that it requires stable information.

2.1.2. Identification Based on Visual Perception

Most works related to RGB-D type sensors [24,25] are limited to extracting characteristics and identifying objects or planes [26–28].

On the other hand, lidar-type sensors are used for re-constructing 3D environments and the semantic identification of areas and objects based on geometries and the extraction of planes and surfaces [29–31]. However, most developments are limited to the extraction of plans [32,33].

Some works use RGB imaging and neural networks for terrain identification, such as [14,34,36–38]. However, there is a lack of systems for detecting and characterizing obstacles or surmountable zones for the robot, which is a fundamental factor for defining walking modes and areas to avoid.

Although the methods based on visual systems are robust and reliable in characterizing the environment, they show some disadvantages. Thus, lidar-based systems cannot infer or provide information about the rigidity or stability of the ground or obstacles.

In this sense, the proposed method seeks to implement a proof of concept by using neural networks trained with a starting criterion of surmountable or non-surmountable obstacles, considering size and location, given by a user.

This first phase consisting of the detection and characterization of terrain allows the robot intelligence systems to develop preliminary strategies to address unstructured environments, by adjusting the modes of locomotion as progress is made, according to the structure of the environment.

2.2. Gait Pattern Adjustment of Bioinspired Quadruped Robots

Biomimetic intelligence systems allow solving complex problems such as moving across complex environments, which is currently of interest at the research level [1].

Some works combine several contact-type sensors to define the displacement of quadruped robots based on the optimization of forces and torque control strategies [39, 40,42]. On the other hand, some developments integrate vision systems to achieve first attempts at traversing terrain with a quadruped robot by using terrain mapping tools in controlled environments [43].

The work “A Review of Quadruped Robots and environment perception” highlights one of the main problems to be addressed within this area, which is the identification of the terrain, which must be interpreted in a bioinspired way to be addressed satisfactorily [44].

There are also other works related to the regulation of gait parameters for robots with legs, such as in ref. [45], which establishes that moving across unstructured terrains with a single gait pattern is complex. This work proposes a system that regulates the gait patterns of a hexapod robot and includes a method based on a fixed gait pattern and an adjustable one based on the inclination of the terrain. In work developed by Zenfer, it is proposed to adjust the gait patterns of a hexapod robot based on the terrain identified by a monocular camera [46].

An analysis of the kinematics of a leg of a quadruped robot is presented in [47]. In [40], one of the first developments in gait pattern regulation is shown, focusing on trot and gallop by using contact sensors on the robot’s legs as feedback.

On the other hand, a method that feeds back the gait patterns of a spider-type robot based on the terrain detected with an RGB-D vision system is proposed in [15]. At the same time, Gong proposes a method for extracting the gait patterns of quadruped animals based on their pose [48]. Chen proposes a method for pattern matching a robot with legs–wheels [49]. A method to adjust the patterns in quadruped robots according to the touchdown times of swing feet is evaluated in [50].

Several relevant works stand out within the state of the art. However, the method proposed by the authors, which combines neural networks to identify the terrain from an RGB image so as to define which obstacles/zones are surmountable, has not been addressed so far to adjust the gait patterns.

3. Methodology

3.1. Materials

The main equipment used for this work is ARTU-R, a quadruped robot, shown in Figure 1. Its sensory system comprises the elements described in Table 1. This robot relies on 12 brushless motors distributed among its four legs to move. The main characteristics of these motors are a weight of 0.605 Kg, a maximum torque of 33.4 N.m and an Encoder of 15 bits used to determine the position of each link.

A Gazebo simulation environment executed in a previous phase on a high-powered computer (MSI-10th Gen, GTX-1660Ti) allows the simulation of different parameters and configurations of movement.



Figure 1. ARTU-R quadruped robot (A1 Rescue Task UPM Robot), equipped with sensory equipment for hostile environments. Numbers on the legs are assigned for identification throughout the manuscript. Source: authors.

Table 1. Materials for the proposed system implementation.

Component	Description
Unitree A1	Quadruped Robot
Nvidia Jetson Xavier-Nx	On-board Embedded System
Real-Sense	RGB-Depth Sensor
MSI1660-Ti Laptop	Computer for Simulations

3.2. Kinematic Modeling of the Legs

The quadruped robot used in this work has three degrees of freedom per leg, which amounts to a total of twelve degrees of freedom. Each limb is made up of three links. The problem will be subdivided into two sections to find the inverse kinematics of the system.

In the first step, the situation of one of the legs in the frontal plane (YZ) in Figure 2a will be analyzed to find the angle q_0 as a function of the distances P_z and P_y and the length L_0 , using Equation (1).

In the second part of the kinematics calculation (Figure 2b), the triangle formed on the limb's lateral side is considered. Thus, it will be possible to obtain the angles q_1 and q_2 from the x and y values. Equations (2) and (3) show the relationship for calculating these angles.

These expressions are found as a function of the parameters of the forward step of the robot given by (h, A) , shown in Figure 2b, that will be combined with the outputs of the neural network to generate the adaptive movement.

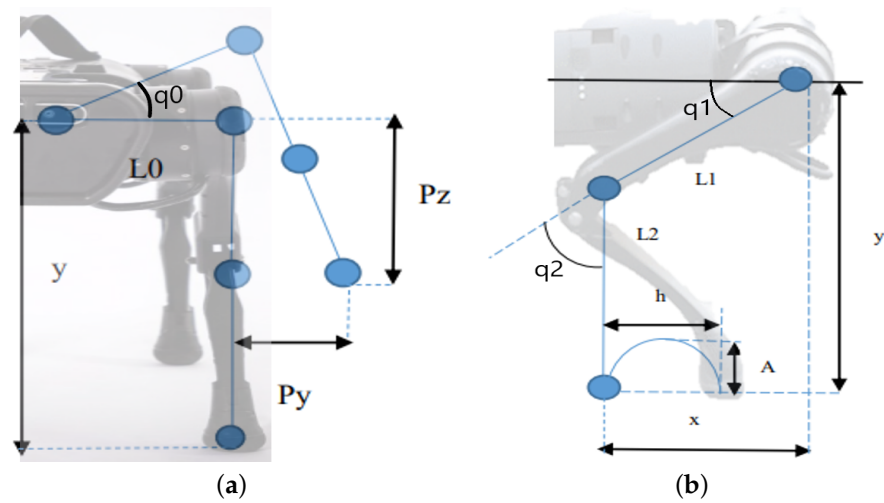


Figure 2. Views and parameters of the kinematic model of the robot. Source: authors. (a) Front view of the kinematic model; (b) lateral view of the kinematic model.

$$q_0 = \tan^{-1}\left(\frac{y_{f(A)}}{L_0}\right) - \tan^{-1}\left(\frac{P_z}{P_y + L_0}\right) \tag{1}$$

$$q_2 = \cos^{-1}\left(\frac{(x_{f(A)})^2 + (y_{f(A)})^2 - L_1^2 - L_2^2}{2 \cdot L_1 \cdot L_2}\right) \tag{2}$$

$$q_1 = \tan^{-1}\left(\frac{y_{f(A)}}{y_{f(h)}}\right) - \tan^{-1}\left(\frac{L_2 \cdot \sin(q_2)}{L_1 - L_2 \cdot \cos(q_2)}\right) \tag{3}$$

Iterative Configuration of Gait Patterns

Once the leg model is obtained, it is adapted to the different base gait patterns analyzed in dogs (Figure 3), where each paw is identified from 1 to 4 according to Figure 1. There are three types of patterns: configuration A, 2-2 alternate, where 1 + 4 and 2 + 3 are moved synchronously; configuration B, 2-2 gallops alternative (movement of 1 + 2 and 3 + 4); and configuration C, 1-3, that has four phases, leaving a support polygon of three legs while the other one is in the air. It is worth noting that the three paws on the ground must continue in a phased synchronous movement to generate an advance. This four-time-phase advance for each leg is illustrated in grayscale for better visualization in Figure 3.

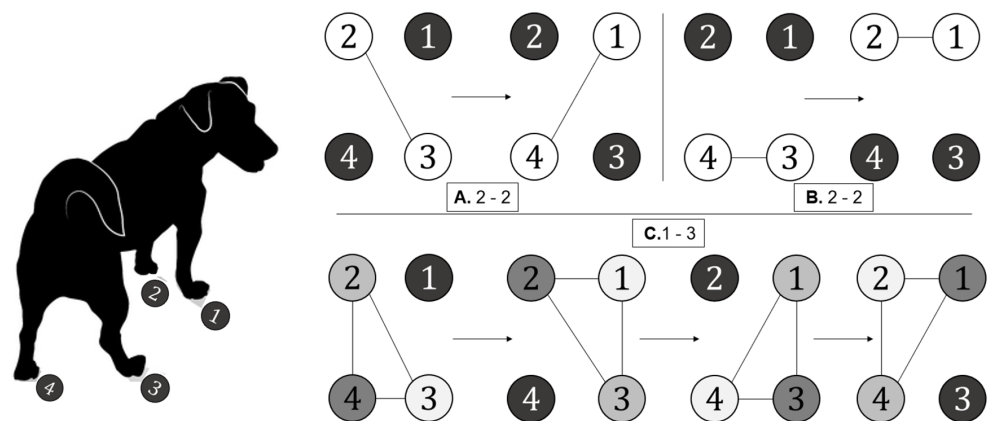


Figure 3. Synthesis of the gait patterns studied. A: 2-2 Altern, B: 2-2 Gallop, and C: 1-3. Source: authors.

The 2-2 gait pattern has great importance. This type of movement has different variants depending on how the two pairs of limbs are organized. On the one hand, there is the alternate mode, in which one front and one hind leg advance simultaneously. In this method, two legs move, leaving the other two static, and later, at the end of the journey of the first one, the other two start-up.

The trajectories to be followed by the hoof have been proposed as a positive sinusoidal curve, with amplitude (A) and half the period equal to the step (h); the parameters shown in Figure 2b.

3.3. Test Environments and Parameters

The simulations carried out in this work have been applied to different types of terrain, all encompassed in the so-called orange sand, according to the Institute of Standards and Technology (NIST). Taking NIST as the regulatory entity, the proposed environments are classified into three types of arenas, yellow, orange and red, each one with a different level of complexity [51]. Accordingly, the scenarios in this work contain moderate obstacles, slight slopes and different consistencies of soils.

3.3.1. Simulated and Real Environments

The simulation phase allows the analysis of the defined gait patterns to evaluate their functionality in unstructured terrain. The ROS-GAZEBO simulator is used, which recreates both the physical and dynamic conditions of the environment. It also allows the integration of the CAD model of the robot with Ros-Control packages.

The simulation in Gazebo is reconstructed based on the CAR-Arena of the UPM to have parity in the concordance of environments. Both environments are shown in Figure 4a,b, respectively. In the same way, outdoor environments are reconstructed for this testing phase according to those used later, shown in Figure 4c,d.

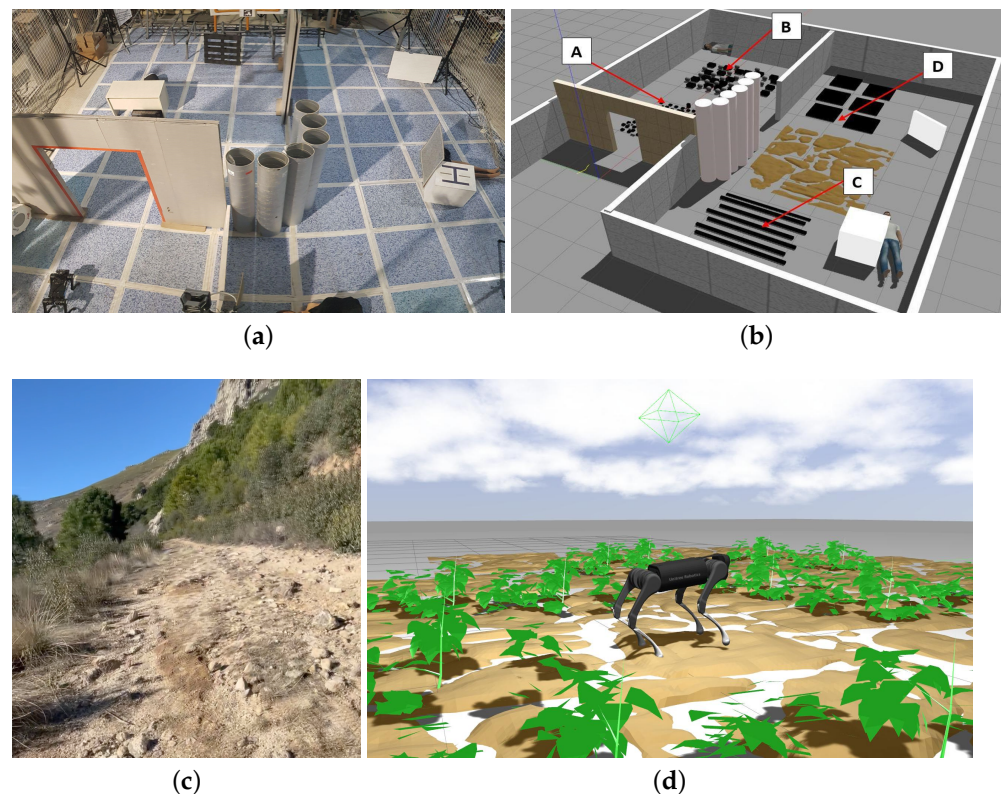


Figure 4. Real and simulated test environments. Source: authors. (a) Real scenario (CAR robotics arena) with different instances for testing; (b) indoor simulated scenario in Gazebo for test execution; (c) outdoor real scenario; (d) outdoor simulated scenario with the robot model.

The indoor environment (Figure 4a,b) consists of different facilities with four types of floors. The first (A), located when crossing the door, has small stone-type rubble that does not exceed 1–3 cm. The second (B), located in the rear-left area, relies on larger rubble pieces (5–9) cm. In the next room, an area (C) with branch-type rubble and an area with unevenness (D) are mainly distinguished.

3.3.2. Type of Tests

A series of tests were carried out in each different type of terrain, analyzing the time required to complete each one of the routes, the stability that the robot shows while facing different obstacles and the maximum distance.

The best gait patterns for each type of scenario and their most appropriate parameters were extracted, and predefined as functions for their extrapolation to the real scenario testing phase.

Tests in real environments are started by identifying the environment and characterizing the debris in terms of size, relative position and distance. Based on these data, the adaptive algorithm for the compensation of the trajectory of the movement of the leg is adjusted for the advance through the terrain. Different kinematic parameters have been analyzed to evaluate the success of each test.

3.4. Convolutional Neural Networks for Identification and Characterization of the Environment

The YOLOv8 convolutional neural network was used to develop this work since it shows several advantages over its predecessors in addition to classification and detection. The main innovative element in this version of CNN is the segmentation layer on the detected objects that it incorporates, which allows extracting more precise information, mainly the centroid, based on the distribution of the specific area of the object.

3.4.1. Datasets and Network Training

The training of the neural network starts with generating a dataset of images captured in outdoor terrain (grass, gravel, and dirt road) with different conditions and various obstacles. The dataset comprises more than 1700 images in the authors' Github repository (Appendix A).

The labeling phase was carried out using the following labels to identify the terrain and the variety of obstacles existing in it: gravel, dirt road, grass, obstacle—surmountable and obstacle—not surmountable.

The dataset was divided into three groups according to the following percentages: training (82%), validation (12%) and testing (6%).

The training phase was carried out on a high-performance computer in the Anaconda environment. The number of epochs required for training was 145. Once the model was obtained, its effectiveness was evaluated in terms of precision, recall and accuracy according to Equations (4)–(6). The components of the true positive (TP), false positive (FP), false negative (FN) and false positive (FP) equations are derived from the inferences in the network detection. These metrics enable the authors to establish curves and analyze elements of the effectiveness of the network, such as the confusion matrix.

$$\text{Precision} = \frac{TP}{TP + FP} \quad (4)$$

$$\text{Recall} = \frac{TP}{TP + FN} \quad (5)$$

$$\text{Accuracy} = \frac{TP + TN}{TP + FP + TN + FN} \quad (6)$$

3.4.2. Automatic Adjustment of Patterns Based on the Neural Network Processing

Figure 5 shows in detail each subsystem of the implementation developed for this work. After the simulation phase, some basic gait patterns able to work in irregular terrain are defined that can work for irregular terrain. The next stage corresponds to adjusting these patterns based on the changing environment.

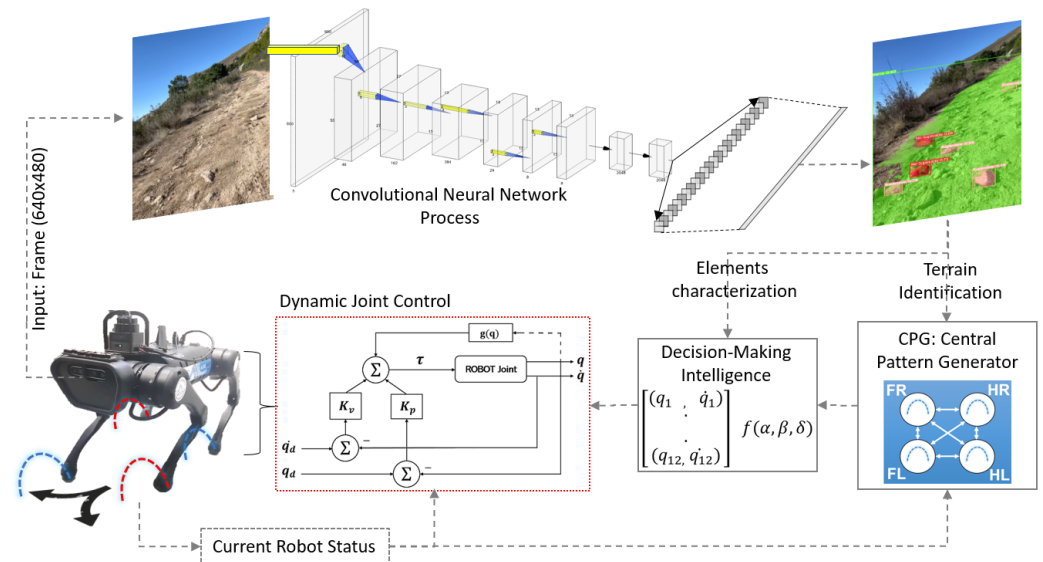


Figure 5. Schematic diagram of the implemented system. Source: authors.

The cyclical process begins with the image captured by the robot. It is processed with the trained model and characteristics of the environment (terrain ID and obstacle characterization) are extracted, which feed the pattern-matching system. The new adjusted values are sent to the predefined dynamic controller of the robot. The computational frequency required for processing all subsystems is 10 Hz.

The parameters provided by the network are, on the one hand, the type of terrain (used to define the basic walking pattern in the Central Pattern Generator—CPG) and, on the other hand, the obstacle list (*Obst*). The centroid (relative to the central position of the camera), radio (*Radio*) and distance (*dist*) are obtained concerning the frame where the robot camera is allocated—in this case, in front of the robot.

Since the number of objects detected could be different for each iteration, and they could be false detections or wrong estimates for the type of terrain, incremental dynamic matrices are used to generate greater confidence in the updating values obtained.

These parameters are used in Equations (7)–(11) to adjust the gait patterns by varying the amplitude and/or its step length according to the dynamic stiffness of the joints. Equations (7) and (9) provide the new values of the marching pattern (A_{temp}, h_{temp}), and Equations (8) and (10) adjust these values in a complementary way to the base pattern due to the identified terrain, together with Equations (1)–(3). Finally, Equation (11) is used to define the stiffness of joint articulations. Algorithm 1 details the functional structure of the process used for the proposed method.

$$(A_{temp}, k_{p1}) = \frac{\sum_{i=1}^n [Obst_{centroid \rightarrow x} + Radio_{Obst \rightarrow Major}] * dist_{Obst}}{n} \tag{7}$$

$$f(A) = A_{def} + (\overline{A_{temp_{def}}}) \tag{8}$$

$$(h_{temp}, k_{p2}) = \frac{\sum_{i=1}^n [Obst_{centroid \rightarrow x} + Radio_{Obst \rightarrow Minor}] * dist_{Obst}}{n} \tag{9}$$

$$f(h) = h_{def} + (\overline{h_{temp_{def}}}) \quad (10)$$

$$K_p = k_{p1} + k_{p2} \quad (11)$$

Algorithm 1 Quadruped Robots Gait Pattern Regulation

```

1: Data:
2:  $im_{RGB} \leftarrow$  RGB image [640x480]
3:  $Robot_{joints-pose} \leftarrow q_{[1-12]}$ 
4:  $Robot_{joints-vel} \leftarrow \dot{q}_{[1-12]}$ 
5:  $Robot_{pose(xyz)-orient(rpy)} \leftarrow IMU_{estimation}$ 
6: Result:
7:  $[q_{d[1-12]}, \dot{q}_{d[1-12]}, \tau_{[1-12]}]$ 
8: function TERRAIN_PROCESSING( $im$ ) ▷ CNN vision-based terrain processing
9:    $CNN_{based-algorithm} \leftarrow im$ 
10:  return  $[Terrain_{ID}, Obstacles_{class,size,pose}]$ 
11: end function
12: function GAIT_PATTERN( $TerrainDetected$ ) ▷ Gait base pattern generator
13:   $[q_{d[1-12]}, \dot{q}_{d[1-12]}, \tau_{[1-12]}] \leftarrow IK_{Solver}_{terrain/exp-based}$ 
14:  return  $[GaitPattern_{[q,\dot{q},\tau]}]$ 
15: end function
16: while  $im_{RGB}$  and  $start$  do ▷ Main Loop
17:    $Robot \leftarrow stand\_position$ 
18:   eval( $TERRAIN\_PROCESSING \leftarrow im_{[RGB]}$ )
19:   if  $Terrain - ID$  not null then
20:     eval ( $GAIT\_PATTERN \leftarrow Terrain - ID$ )
21:     if  $Obstacles$  in  $terrain$  not null then
22:       eval_adjusted_pattern( $[f(A), f(h), K_p] \leftarrow Obstacles_{[number,pose,size]}$ )
23:       update_control_variables( $[q_{d[1-12]}, \dot{q}_{d[1-12]}, \tau_{[1-12]}] \leftarrow [f(A), f(h), K_p]$ )
24:        $Robot_{Controller} \leftarrow [q_{d[1-12]}, \dot{q}_{d[1-12]}, \tau_{[1-12]}]$ 
25:     else
26:        $Robot_{Controller} \leftarrow [q_{d[1-12]}, \dot{q}_{d[1-12]}, \tau_{[1-12]}]$ 
27:     end if
28:   else
29:      $Robot \leftarrow stand\_position$ 
30:   end if
31: end while

```

A PD (proportional-derivative) controller with gravity compensation is used for each joint. One of the most responsive parameters is the constant K_p or stiffness constant since the behavior of the entire leg in front of an obstacle depends on the magnitude. Thus, if high K_p values are set, a small margin to generate adaptability in the face of the obstacle is obtained. Due to this, K_p values are specified for each joint at every step in order to obtain adequate adaptability. These values are directly proportional to the number of obstacles and environment.

4. Results

4.1. Simulation Analysis

In the first part of validating the implemented method, the three types of gait pattern are evaluated on the different scars (Simulator Common Architecture Requirements Standards) in simulation to define the best initial set-up as the basis for transfer learning. Figure 6 shows the results of the simulations, where the robot model can be seen moving in the different scenarios. The hoof trajectory corresponding to each gait pattern is shown in blue.

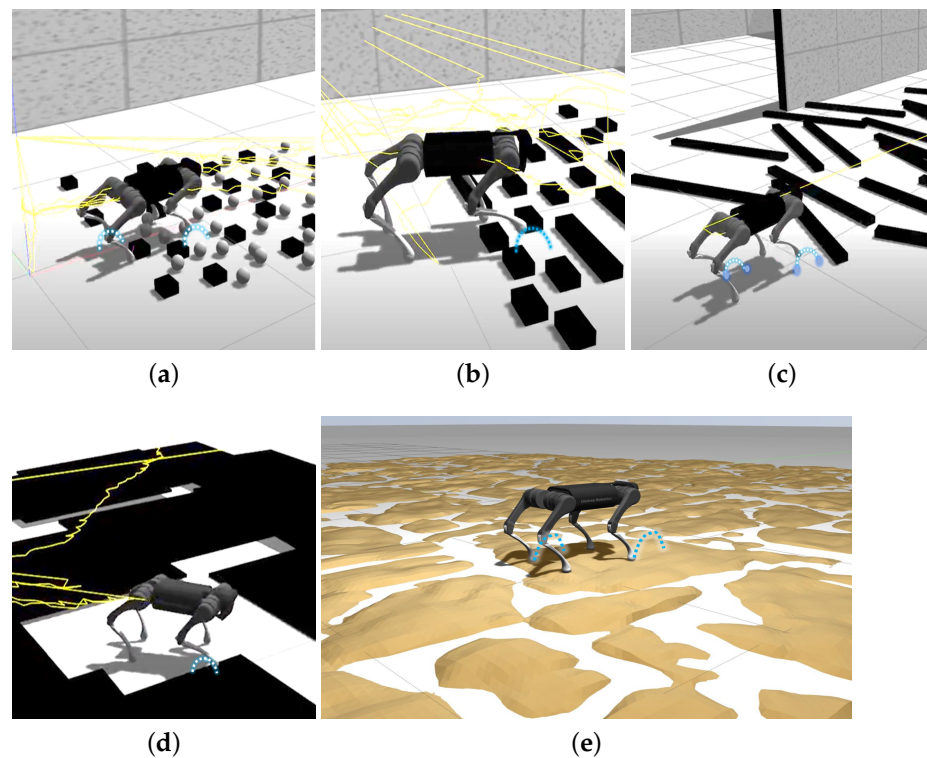


Figure 6. Tests executed in simulation. The trajectory described by the end of the robot’s leg is shown in blue. Source: authors. (a) Conf: 2-2 Debris: small. (b) Conf: 1-3 Debris: medium. (c) Conf: 2-2 Debris: branches. (d) Conf: 1-3 Unevenness. (e) Conf: 1-3 Unevenness.

Figure 6a shows the Gazebo simulation on terrain with small prismatic and spherical obstacles, corresponding to the type of soil (A) detailed in Section 3.3.2. It is found that the most favorable gait pattern for this soil is 2-2. The average time for the robot to reach the goal in this scenario is 14.2 s.

Figure 6b–e show the rest of the tests carried out. Table 2 summarizes the results of the tests carried out in terms of time, percentage progress and distance covered.

Table 2. Gazebo simulation results.

Scenario:		Simulation Results			
Gait Patterns	Repetitions:	A.	B.	C.	D.
		30	30	30	30
1-3	av. time (s)	18.2	21.1	17.7	48.3
	% advance	98.3	90.2	66.3	75.3
	av. distance (m)	3.4	1.9	2.9	3.9
2-2 alternate	av. time (s)	14.2	10.2	16.3	17.4
	% advance	98.4	98.1	73.2	81.5
	av. distance (m)	3.3	2.1	2.41	4.41
2-2 gallop	av. time (s)	25.1	9.2	14.6	13.6
	% advance	81.4	54.4	64.1	75.5
	av. distance (m)	2.3	2.1	2.41	3.41

The most appropriate gait mode is the so-called alternate 2-2. When following a 1-3 pattern, the robot is able to advance but cannot fully overcome the obstacles. Moreover, the 2-2 gallop mode turned out to not be the most suitable for this type of scenario.

Accordingly, the alternate 2-2 mode is used as a base pattern for the tests carried out with the real robot; the adjustment of this pattern will be simultaneously executed based on the perceptible environment of the robot.

4.2. Evaluation of Detection and Autonomous Characterization of Real Terrain

4.2.1. Analysis of the Convolutional Neural Network Efficiency

Figure 7a shows the confusion matrix for the trained model of the neural network. The main diagonal shows high values close to one, indicating a high confidence level for detecting each class.

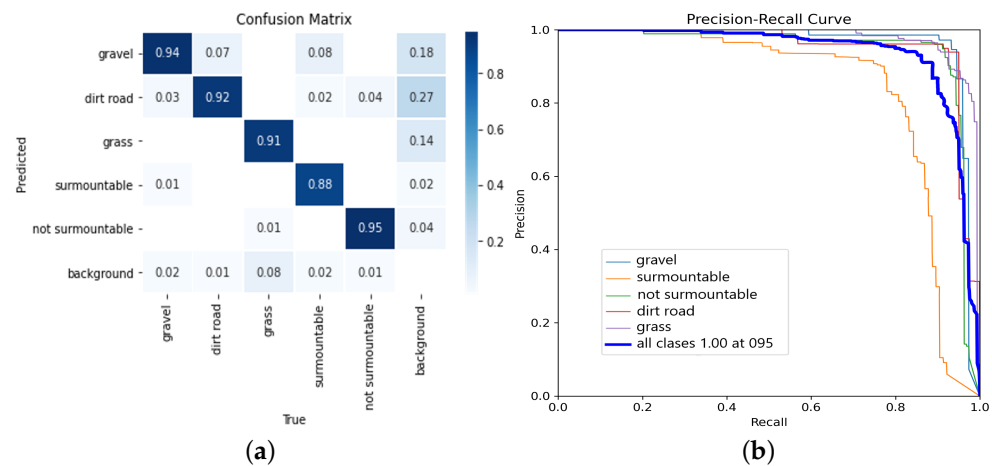


Figure 7. Evaluation of the trained neural network model. Source: authors. (a) Confusion matrix for the trained model. (b) Precision–recall curve for the trained model.

The best identification rate was obtained for the terrain with gravel. In the same way, the obstacles that cannot be overcome are well identified (95%), a significant factor that acknowledges that due to the geometric restrictions of the robot or the arrangement of the obstacle in the environment, it cannot be overcome, and reactive movements are generated to avoid it.

On the other hand, Figure 7b shows the precision–recall curve, which shows the trend of stability in detection precision and its subsequent decline. The values obtained for all the classes are uniform and over 90%, except for the class of surmountable obstacles, which provides a value of 88%.

4.2.2. Evaluation of the Environment Characterization

The evaluation results for the outdoor scenarios are illustrated in Figure 8. This figure shows the different overlapping layers on the analyzed image, the bounding boxes, the classes and the precision percentages for each detected obstacle.

Figure 8a shows a first environment with grassy soil, segmented in green with different obstacles. Those that can be overcome are shown in pink, and those that cannot be overcome due to their size or instability in red. The areas detected for both environment and obstacles have a high efficiency. This is mainly because the environment is quite structured, similar to the one in Figure 8b (gravel).

On the other hand, Figure 8c–e correspond to terrains with rough conditions, where both terrain and obstacles are marked as layers of colors. In these cases, the percentage of success in detection and characterization also obtains a high confidence index in the implemented method.

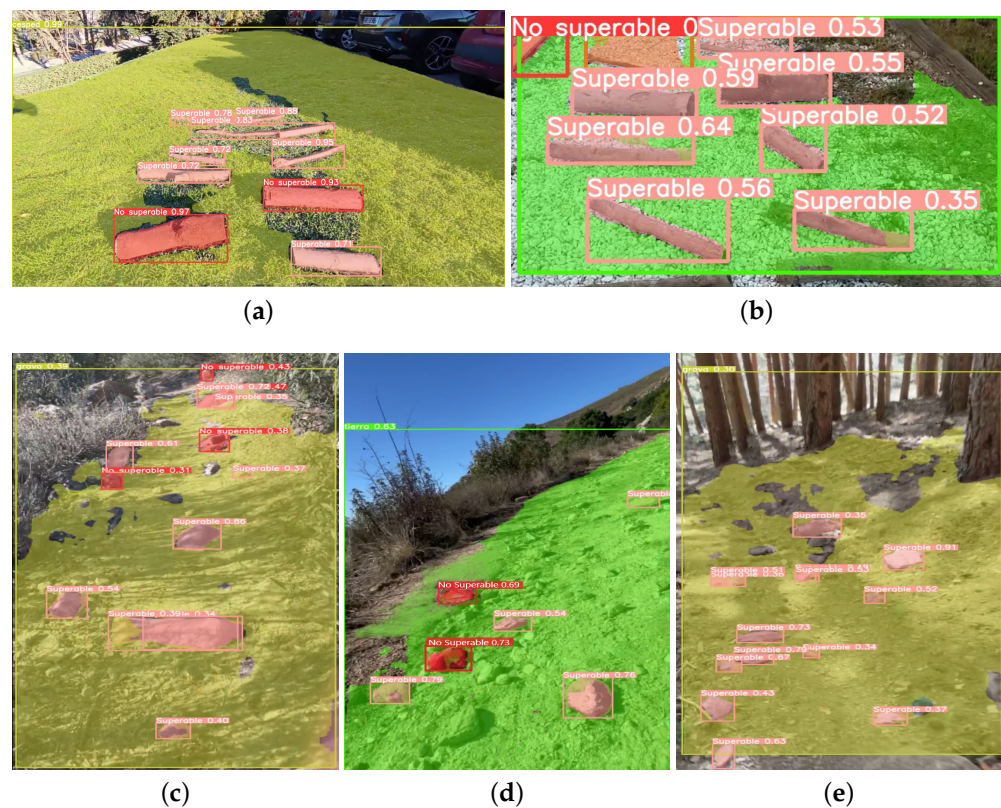


Figure 8. Analysis of the terrain characterization through the trained neural network. Source: authors. (a) Outdoor scenario analysis—grass with obstacles. (b) Outdoor scenario analysis—gravel with obstacles. (c) Outdoor scenario analysis—dirt road with obstacles. (d) Outdoor scenario analysis—gravel with obstacles. (e) Outdoor scenario analysis—dirt road obstacles.

4.2.3. Analysis of the Vision Method Regarding the State of the Art

The most important benchmarks that contain images of outdoor environments and semantic segmentation of the terrain are MSeg [52], TAS-NIR [53], TAS500 [54], TimberSeg [55] and RELIS-3D [56].

Most of these benchmarks directly catalog the terrain as “roads”, “sidewalks” or “vegetation” but do not go into detail about the type of terrain or what it is, or more specific characteristics that it may contain, such as obstacles. The rest of the tags generalize urban environments in a certain way, such as traffic light, traffic sign, vegetation, terrain, sky, person, rider, car, etc.

For the development of this approach, different external scenarios corresponding to the [54,55] benchmarks are evaluated using the introduced neural network model to verify its effectiveness. The main results obtained are related to both the terrain detected and the presence of obstacles, as well as the percentage of terrain segmentation concerning the benchmark.

Figure 9 shows the result of detecting terrain type and semantic segmentation. However, elements such as the sky, people or cars are not detected. It should be noted that the model is not focused on that type of element, only on the ground and possible obstacles. Figure 9a,b shows the correct identification of the soil (grass) with an average precision of 0.88% and 0.94% of the total segmented area concerning the original benchmark.

On the other hand, Figure 9c,d shows the recognition of the soil, identified as gravel, and in the first case, an obstacle identified as surmountable. In the second case, the bushes are identified as obstacles. However, these are outside the identified terrain, so they are not part of the displacement environment. In both cases, the average percentage of detection of the segmented space concerning the benchmark is 93%.

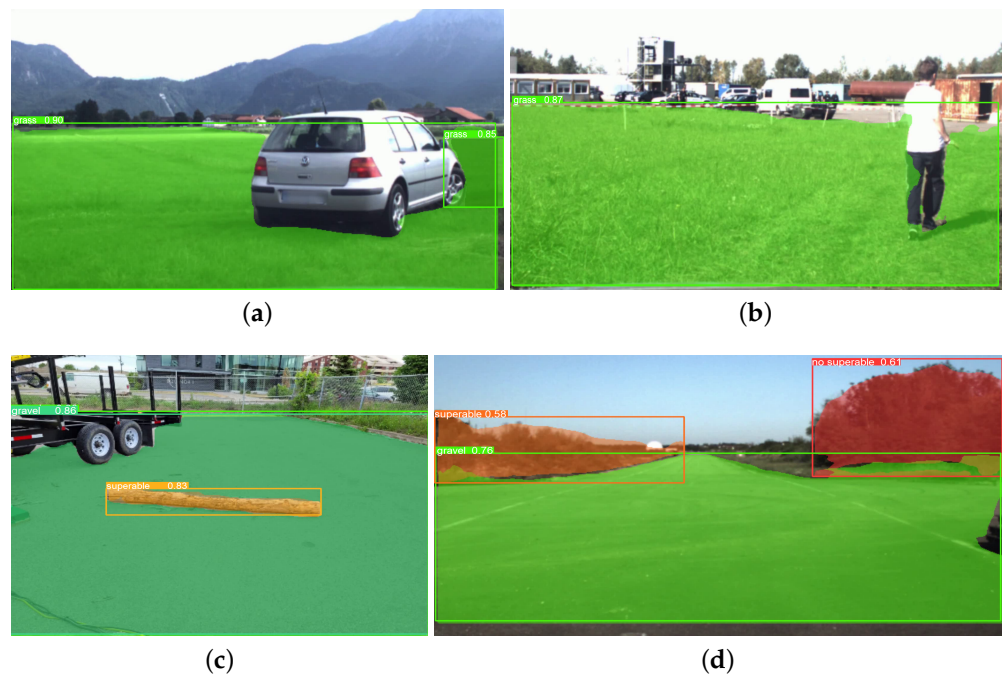


Figure 9. Evaluation of the trained neural network model over datasets [54,55] for terrain and obstacle detection. Source: authors. (a) Evaluation of terrain with the proposed detection model on the dataset [54]. (b) Evaluation of terrain with the proposed detection model on the dataset [54]. (c) Evaluation of terrain and obstacles with the proposed detection model on the dataset [55]. (d) Evaluation of terrain and obstacles with the proposed detection model on the dataset [55].

On the other hand, a comparison is established, based on different metrics of the proposed method against those existing in the state-of-the-art vision system for land characterization. This approach is shown in detail in Table 3 and shows the strengths of the proposed method.

Table 3. Comparison of the proposed method for terrain identification characterization concerning state-of-the-art methods. Meets: ✓. Fails: X.

Work	Terrain ID	Obstacle ID	Benchmark Test	Sensor	Tested on Robots	Semantic Segmentation
[?]	✓	X	X	RGB	X	X
[14]	✓	X	✓	RGB-D	✓	X
[34]	✓	X	✓	RGB	X	✓
[36]	✓	X	X	RGB	X	✓
[15]	✓	X	X	RGB-D	✓	X
[46]	✓	X	✓	RGB	✓	X
[16]	✓	X	X	RGB	X	X
[37]	✓	X	X	RGB-D	✓	✓
[57]	✓	X	X	RGB	✓	✓
[25]	X	✓	X	stereo camera	✓	X
[38]	✓	X	X	RGB	X	✓
Authors	✓	✓	✓	RGB-D	✓	✓

As the first result of this comparison, it can be established that most of the previously developed works were focused on the characterization of the terrain, either with a subsequent step of semantic segmentation or not. Moreover, there is a lack of systems for characterizing components such as debris, information that is valuable for decision making in the field of outdoor robotics.

Other conventional methods for environment identification based on point clouds generally use traversability maps [58,59]. However, this method lacks relevant environmental information, such as the stability of areas and obstacles. Identifying terrains using the proposed method provides a better perception of the environment and its stability. Using traversability maps, the environment is considered compact, and pass/no-pass zones are established to generate planning routes based on different heights or slopes.

4.3. Analysis of Results Working with the Real Robot

Tests were carried out mainly in outdoor environments to validate the joint operation of the proposed method. Figure 10 shows three scenarios where the tests were carried out. For the quantitative evaluation, an advance of two meters is considered. The initial points are marked with the number one, the intermediate steps as two and the final point as three.



(a)



(b)



(c)

Figure 10. Evaluation of the robot's performance in overcoming different types of terrain. Source: authors. (a) Overcoming of external terrain, type dirt road. (b) Overcoming of external terrain with obstacles. (c) Overcoming of external terrain, type gravel.

Figure 10a corresponds to a dirt-road-type terrain. Figure 10b shows a scenario with several obstacles to overcome, while Figure 10a corresponds to a terrain with gravel. In the three scenarios, different superimposed frames of the robot moving along the path are shown.

Tables 4 and 5 show the results corresponding to a series of tests carried out on different terrains, both with and without obstacles, respectively. It can be seen (as preliminary conclusions from these results) that the influence of terrain with obstacles increases the time required to complete the mission since the speed of the robot decreases. On the other hand, the pattern adjustment algorithm increases the mean values of the gait pattern to overcome these detected obstacles. Although the percentage of success decreases, the average pass rate for these areas is over 90.5%. This demonstrates the proposed method's effectiveness in addressing unstructured terrain in this first approximation.

Table 4. Test results for a two-meter course on terrain with obstacles.

Scenery	Dirt Road	Compact Soil	Gravel	Grass
Number of Tests	15	12	12	12
Mean speed	0.09 m/s	0.11 m/s	0.11 m/s	0.12 m/s
Mean time	20.1 s	17.1 s	17.7 s	16.3 s
Average body height	23.1 cm	23.2 cm	22.1 cm	22.9 cm
Average step height (A)	14.7 cm	13.2 cm	14.7 cm	12.6 cm
Average step length (h)	6.5 cm	7.0 cm	7.1 cm	6.8 cm
Completion success rate	89%	91%	89%	93%

Table 5. Test results for a two-meter run on unstructured terrain.

Scenery	Dirt Road	Compact Soil	Gravel	Grass
Number of tests	15	15	15	10
Mean speed	0.19 m/s	0.23 m/s	0.2 m/s	0.19 m/s
Mean time	10.2 s	8.5 s	9.7 s	10.2 s
Average body height	25.6 cm	25.3 cm	23.1 cm	24.4 cm
Average step height (A)	10.7 cm	8.4 cm	10.7 cm	9.3 cm
Average step length (h)	7.3 cm	8.1 cm	9.1 cm	7.9 cm
Completion success rate	94%	100%	93%	100%

Comparison of Gait Pattern Adjustment Methods in the State of the Art

The developed comparison is shown in Table 6. The previously developed works focused on adjusting the gait patterns of different types of robots, not only quadrupedal ones. Those referring to quadruped robots mostly use the adjustment of patterns using contact sensors with the floor to evaluate the stability in an all/nothing way. Some other works already integrate RGB-D image processing to characterize the spatial depth in each step to adjust the march.

Table 6. Comparison of gait pattern adjustment methods. Meets: ✓. Fails: X.

Work	Robot	Visual Terr. Det.	Visual Obst Det.	Pattern	Test Real/Sim
[40]	Quadruped	X	X	2-2/3-1	Real
[45]	Hexapod	X	X	alternate tripod	Sim
[47]	Quadruped	X	X	2-2	Study
[15]	Spider	✓	X	alternate pairs	Real
[46]	Spider	✓	X	tripod	Real
[12]	Hexapod	X	X	tripod	Real
[48]	-	X	X	pattern extraction	Real
[49]	wheel-legged	X	✓	hybrid	Real
[50]	Quadruped	X	X	2-2	Sim
[43]	Quadruped	X	✓	2-2	Real
Authors	Quadruped	✓	✓	2-2/3-1	Real/Sim

On the other hand, several works based on hexapod and spider robots are able to regulate their gait patterns (mostly alternate tripod) depending on the type of terrain using RGB sensors. However, a development similar to the proposed by the authors for

regulating gait patterns based on visual processing and characterizing the environment has not been found in a specific way.

4.4. Joint Behavior

Figure 11 shows the results of the joint behavior (angular position, velocity and torque) during the initial 10 seconds of displacement across the terrain test with obstacles in Figure 10. The units and nomenclature are described as position (Pos) (rad) (blue), velocity (Vel) (rad/s) (orange – scale * 0.1) and torque (Trq) (N.m) (green – scale * 0.01) of the joints.

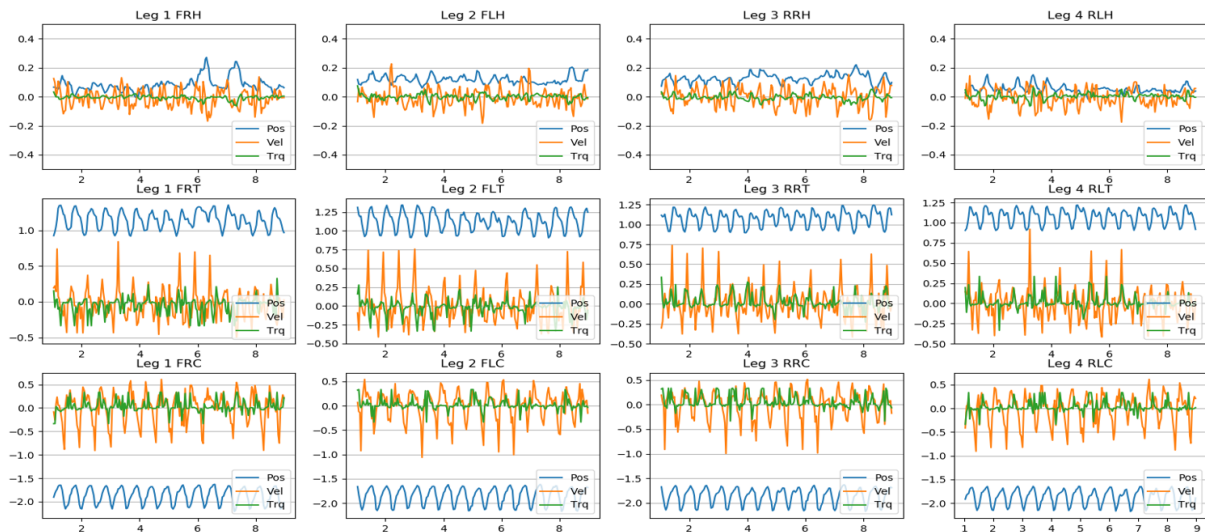


Figure 11. Joint behavior compared to the 2-2 configuration gait pattern with high amplitude (14 cm) and medium footprint (5 cm), for a dirt-road-type environment with obstacles for time $t = 10$ s.

The graphs show the behavior of each of the three joints, corresponding to the four limbs, according to the nomenclature in Table 7.

Table 7. Robot joint nomenclature.

Joint Nomenclature					
1. F	Front	2. R	Right	3. H	Hip
				3. T	Thigh
1. R	Rear	2. L	Left	3. C	Calf

The oscillatory movement of the position can be highlighted especially in the thigh and calf joints, which generate progress according to the gait pattern. In contrast, the joint behavior of the hip position is more uniform. In the same way, the velocity graphs have similar oscillatory behavior in the same type of position.

There are notable variations, especially in the 6–8 s for the front legs. These variations are due to the obstacles in the environment, which prevent reaching the movement’s referential positions. The hip joint’s movement stands out, which acts in a reactive manner to adapt to the variability of the terrain.

5. Conclusions

In this article, a method is presented and validated to overcome unstructured terrain using a quadruped robot. This method uses robot-modeled gait patterns and automatic identification–characterization of the environment to adjust these gait patterns automatically.

The study of bio-inspired locomotion systems in quadruped animals has allowed their imitation by real robots. These movements and gait patterns have been combined with intelligent systems to adjust movement in unstructured environments. This knowledge is used for the initial training of neural networks, which has allowed carrying out successful displacement in unstructured terrain with the robot.

The simulation phase has allowed validating the imitation of the gait patterns of dogs and analyzing their effectiveness in different types of terrain with obstacles. In this way, the 2-2 alternate type of gait pattern is revealed as the most adequate to overcome environments with debris. This pattern is considered to feed into the central gait pattern generator, which serves as the basis for forward movements.

The autonomous visual identification of the terrain and the characterization of the obstacles using convolutional neural networks has shown high efficiency, with a high percentage of precision (>90%) in the location of obstacles in real dynamic environments. This method is compared with similar state-of-the-art and relevant benchmarks, obtaining optimal functionality results.

The proposed method offers an enhanced understanding of the environment and its stability for terrain identification by utilizing RGB images. In contrast, conventional approaches relying on point clouds often require traversability maps. Nevertheless, these maps suffer from a lack of environmental details, including area stability and obstacle information.

The proposed method based on vision has shown operation efficiency outdoors. It could be extrapolated to other robotic systems and autonomous navigation vehicles. Future lines of research and subsequent developments based on sensory fusion with lidar systems to obtain more precise measurements of the characterized environment could be delivered from it.

Author Contributions: Conceptualization, A.B., L.S., C.C.U. and J.D.C.; methodology, A.B. and C.C.U.; software, L.S. and C.C.U.; validation, L.S. and C.C.U.; formal analysis, L.S., C.C.U. and A.B.; investigation, L.S., C.C.U., A.B. and J.D.C.; resources, A.B. and J.D.C.; data curation, L.S. and C.C.U.; writing—original draft preparation, L.S., C.C.U. and J.D.C.; writing—review and editing, L.S., C.C.U. and A.B.; visualization, C.C.U., A.B. and J.D.C.; supervision, C.C.U., A.B. and J.D.C.; project administration, A.B. and J.D.C.; funding acquisition, A.B. and J.D.C. All authors have read and agreed to the published version of the manuscript.

Funding: This research was made possible thanks to the financing of RoboCity2030-DIH-CM, Madrid Robotics Digital Innovation Hub, S2018/NMT-4331, funded by “Programas de Actividades I+D en la Comunidad Madrid” and cofunded by Structural Funds of the EU and TASAR (Team of Advanced Search And Rescue Robots), in the project “Proyectos de I+D+i del Ministerio de Ciencia, Innovación y Universidades” (PID2019-105808RB-I00). This research was developed in Centro de Automática y Robótica—Universidad Politécnica de Madrid—Consejo Superior de Investigaciones Científicas (CAR UPM-CSIC).

Institutional Review Board Statement: Not applicable.

Data Availability Statement: The dataset for neural network training can be found in Appendix A.

Conflicts of Interest: The authors declare no conflict of interest.

Abbreviations

The following abbreviations are used in this manuscript:

ARTU-R	A1 Rescue Task UPM—Robot
ROS	Robot Operating System
CNN	Convolutional Neural Network
YOLO	You Only Look Once

Appendix A

The dataset used in Neural Network Training can be found through the following link: <https://github.com/ChristyanCruz11/Terrains> (accessed on 1 June 2023).

References

1. Wang, J.; Chen, W.; Xiao, X.; Xu, Y.; Li, C.; Jia, X.; Meng, M.Q.H. A survey of the development of biomimetic intelligence and robotics. *Biomim. Intell. Robot.* **2021**, *1*, 100001. [[CrossRef](#)]
2. Moro, F.L.; Spröwitz, A.; Tuleu, A.; Vespignani, M.; Tsagarakis, N.G.; Ijspeert, A.J.; Caldwell, D.G. Horse-like walking, trotting, and galloping derived from kinematic Motion Primitives (kMPs) and their application to walk/trot transitions in a compliant quadruped robot. *Biol. Cybern.* **2013**, *107*, 309–320. [[CrossRef](#)]
3. Pettersen, K.Y. Snake robots. *Annu. Rev. Control* **2017**, *44*, 19–44. [[CrossRef](#)]
4. Murphy, R.R. *Disaster Robotics*; MIT Press: Cambridge, MA, USA, 2014.
5. Wannous, C.; Velasquez, G. United Nations Office for Disaster Risk Reduction (UNISDR)—UNISDR’s Contribution to Science and Technology for Disaster Risk Reduction and the Role of the International Consortium on Landslides (ICL). In *Advancing Culture of Living with Landslides*; Sassa, K., Mikoš, M., Yin, Y., Eds.; Springer International Publishing: Cham, Switzerland, 2017; pp. 109–115.
6. Blackburn, M.R.; Everett, H.R.; Laird, R.T. *After Action Report to the Joint Program Office: Center for the Robotic Assisted Search and Rescue (CRASAR) Related Efforts at the World Trade Center*; Technical Report; Space and Naval Warfare Systems Center: San Diego, CA, USA, 2002.
7. Eguchi, R.; KenElwood.; Lee, E.K.; Greene, M. *The 2010 Canterbury and 2011 Christchurch New Zealand Earthquakes and the 2011 Tohoku Japan Earthquake*; Technical Report; Earthquake Engineering Research Institute: Berkeley, CA, USA, 2012.
8. Kruijff, I.; Freda, L.; Gianni, M.; Ntouskos, V.; Hlavac, V.; Kubelka, V.; Zimmermann, E.; Surmann, H.; Dulic, K.; Rottner, W.; et al. Deployment of ground and aerial robots in earthquake-struck Amatrice in Italy (brief report). In Proceedings of the 2016 IEEE International Symposium on Safety, Security, and Rescue Robotics (SSRR), Lausanne, Switzerland, 23–27 October 2016; pp. 278–279. [[CrossRef](#)]
9. Whitman, J.; Zevallos, N.; Travers, M.; Choset, H. Snake Robot Urban Search After the 2017 Mexico City Earthquake. In Proceedings of the 2018 IEEE International Symposium on Safety, Security, and Rescue Robotics (SSRR), Philadelphia, PA, USA, 6–8 August 2018; pp. 1–6. [[CrossRef](#)]
10. Chai, H.; Li, Y.; Song, R.; Zhang, G.; Zhang, Q.; Liu, S.; Hou, J.; Xin, Y.; Yuan, M.; Zhang, G.; et al. A survey of the development of quadruped robots: Joint configuration, dynamic locomotion control method and mobile manipulation approach. *Biomim. Intell. Robot.* **2022**, *2*, 100029. [[CrossRef](#)]
11. Meng, X.; Cao, Z.; Zhang, L.; Wang, S.; Zhou, C. A slope detection method based on 3D LiDAR suitable for quadruped robots. In Proceedings of the 2016 12th World Congress on Intelligent Control and Automation (WCICA), Guilin, China, 12–15 June 2016; pp. 1398–1402. [[CrossRef](#)]
12. Wu, X.A.; Huh, T.M.; Sabin, A.; Suresh, S.A.; Cutkosky, M.R. Tactile Sensing and Terrain-Based Gait Control for Small Legged Robots. *IEEE Trans. Robot.* **2020**, *36*, 15–27. [[CrossRef](#)]
13. Giguere, P.; Dudek, G. A Simple Tactile Probe for Surface Identification by Mobile Robots. *IEEE Trans. Robot.* **2011**, *27*, 534–544. [[CrossRef](#)]
14. Vulpi, F.; Milella, A.; Marani, R.; Reina, G. Recurrent and convolutional neural networks for deep terrain classification by autonomous robots. *J. Terramech.* **2021**, *96*, 119–131. [[CrossRef](#)]
15. Walas, K. Terrain classification and negotiation with a walking robot. *J. Intell. Robot. Syst.* **2015**, *78*, 401–423. [[CrossRef](#)]
16. Angelova, A.; Matthies, L.; Helmick, D.; Perona, P. Fast Terrain Classification Using Variable-Length Representation for Autonomous Navigation. In Proceedings of the 2007 IEEE Conference on Computer Vision and Pattern Recognition, Minneapolis, MN, USA, 17–22 June 2007; pp. 1–8. [[CrossRef](#)]
17. Nampoothiri, M.H.; Vinayakumar, B.; Sunny, Y.; Antony, R. Recent developments in terrain identification, classification, parameter estimation for the navigation of autonomous robots. *SN Appl. Sci.* **2021**, *3*, 480. [[CrossRef](#)]
18. Giguere, P.; Dudek, G. Surface identification using simple contact dynamics for mobile robots. In Proceedings of the 2009 IEEE International Conference on Robotics and Automation, Kobe, Japan, 12–17 May 2009; pp. 3301–3306. [[CrossRef](#)]
19. Aggarwal, A.; Kirchner, F. Object Recognition and Localization: The Role of Tactile Sensors. *Sensors* **2014**, *14*, 3227–3266. [[CrossRef](#)]
20. Schmidt, A.; Walas, K. The Classification of the Terrain by a Hexapod Robot. In Proceedings of the 8th International Conference on Computer Recognition Systems CORES 2013, Milkow, Poland, 27–29 May 2013; Burduk, R., Jackowski, K., Kurzynski, M., Wozniak, M., Zolnierak, A., Eds.; Springer International Publishing: Heidelberg, Germany, 2013; pp. 825–833.
21. Brooks, C.; Iagnemma, K. Vibration-based terrain classification for planetary exploration rovers. *IEEE Trans. Robot.* **2005**, *21*, 1185–1191. [[CrossRef](#)]
22. Legnemma, K.; Brooks, C.; Dubowsky, S. Visual, tactile, and vibration-based terrain analysis for planetary rovers. In Proceedings of the 2004 IEEE Aerospace Conference Proceedings (IEEE Cat. No.04TH8720), Big Sky, MT, USA, 6–13 March 2004; Volume 2, pp. 841–848. [[CrossRef](#)]

23. Bai, C.; Guo, J.; Zheng, H. Three-Dimensional Vibration-Based Terrain Classification for Mobile Robots. *IEEE Access* **2019**, *7*, 63485–63492. [[CrossRef](#)]
24. Gupta, S.; Girshick, R.; Arbeláez, P.; Malik, J. Learning Rich Features from RGB-D Images for Object Detection and Segmentation. In Proceedings of the Computer Vision—ECCV 2014, Zurich, Switzerland, 6–12 September 2014; Fleet, D., Pajdla, T., Schiele, B., Tuytelaars, T., Eds.; Springer International Publishing: Cham, Switzerland, 2014; pp. 345–360.
25. Manduchi, R.; Castano, A.; Talukder, A.; Matthies, L. Obstacle detection and terrain classification for autonomous off-road navigation. *Auton. Robot.* **2005**, *18*, 81–102. [[CrossRef](#)]
26. Cruz, C.; del Cerro, J.; Barrientos, A. Mixed-reality for quadruped-robotic guidance in SAR tasks. *J. Comput. Des. Eng.* **2023**, *6*. [[CrossRef](#)]
27. Kırçali, D.; Tek, F.B. Ground Plane Detection Using an RGB-D Sensor. In *Information Sciences and Systems 2014, Proceedings of the 29th International Symposium on Computer and Information Sciences, Krakow, Poland, 27–28 October 2014*; Czachórski, T., Gelenbe, E., Lent, R., Eds.; Springer International Publishing: Cham, Switzerland, 2014; pp. 69–77.
28. Asif, U.; Bennamoun, M.; Sohel, F.A. RGB-D Object Recognition and Grasp Detection Using Hierarchical Cascaded Forests. *IEEE Trans. Robot.* **2017**, *33*, 547–564. [[CrossRef](#)]
29. Ye, X.; Li, J.; Huang, H.; Du, L.; Zhang, X. 3D Recurrent Neural Networks with Context Fusion for Point Cloud Semantic Segmentation. In Proceedings of the European Conference on Computer Vision (ECCV), Munich, Germany, 8–14 September 2018.
30. McDaniel, M.W.; Nishihata, T.; Brooks, C.A.; Iagnemma, K. Ground plane identification using LIDAR in forested environments. In Proceedings of the 2010 IEEE International Conference on Robotics and Automation, Anchorage, AK, USA, 3–7 May 2010; pp. 3831–3836. [[CrossRef](#)]
31. Douillard, B.; Underwood, J.; Kuntz, N.; Vlaskine, V.; Quadros, A.; Morton, P.; Frenkel, A. On the segmentation of 3D LIDAR point clouds. In Proceedings of the 2011 IEEE International Conference on Robotics and Automation, Shanghai, China, 9–13 May 2011; pp. 2798–2805. [[CrossRef](#)]
32. Pomares, A.; Martínez, J.L.; Mandow, A.; Martínez, M.A.; Morán, M.; Morales, J. Ground Extraction from 3D Lidar Point Clouds with the Classification Learner App. In Proceedings of the 2018 26th Mediterranean Conference on Control and Automation (MED), Zadar, Croatia, 19–22 June 2018; pp. 1–9. [[CrossRef](#)]
33. Choi, S.; Park, J.; Byun, J.; Yu, W. Robust ground plane detection from 3D point clouds. In Proceedings of the 2014 14th International Conference on Control, Automation and Systems (ICCAS 2014), Gyeonggi-do, Republic of Korea, 22–25 October 2014; pp. 1076–1081. [[CrossRef](#)]
34. Zhang, W.; Chen, Q.; Zhang, W.; He, X. Long-range terrain perception using convolutional neural networks. *Neurocomputing* **2018**, *275*, 781–787. [[CrossRef](#)]
41. Wang, W.; Zhang, B.; Wu, K.; Chepinskiy, S.A.; Zhilenkov, A.A.; Chernyi, S.; Krasnov, A.Y. A visual terrain classification method for mobile robots' navigation based on convolutional neural network and support vector machine. *Trans. Inst. Meas. Control* **2022**, *44*, 744–753.
36. Verbickas, R.; Whitehead, A. Sky and ground detection using convolutional neural networks. In Proceedings of the International Conference on Machine Vision and Machine Learning (MVML), Prague, Czech Republic, 14–15 August 2014; Volume 1.
37. Brandão, M.; Shiguematsu, Y.M.; Hashimoto, K.; Takanishi, A. Material recognition CNNs and hierarchical planning for biped robot locomotion on slippery terrain. In Proceedings of the 2016 IEEE-RAS 16th International Conference on Humanoid Robots (Humanoids), Cancun, Mexico, 15–17 November 2016; pp. 81–88. [[CrossRef](#)]
38. Kozłowski, P.; Walas, K. Deep neural networks for terrain recognition task. In Proceedings of the 2018 Baltic URSI Symposium (URSI), Poznan, Poland, 15–17 May 2018; pp. 283–286. [[CrossRef](#)]
39. Valsecchi, G.; Grandia, R.; Hutter, M. Quadrupedal Locomotion on Uneven Terrain With Sensorized Feet. *IEEE Robot. Autom. Lett.* **2020**, *5*, 1548–1555. [[CrossRef](#)]
40. Gehring, C.; Coros, S.; Hutter, M.; Bloesch, M.; Hoepflinger, M.A.; Siegwart, R. Control of dynamic gaits for a quadrupedal robot. In Proceedings of the 2013 IEEE International Conference on Robotics and Automation, Karlsruhe, Germany, 6–10 May 2013; pp. 3287–3292. [[CrossRef](#)]
41. Sprowitz, A.; Tuleu, A.; Vespignani, M.; Ajallooeian, M.; Badri, E.; Ijspeert, A.J. Towards dynamic trot gait locomotion: Design, control, and experiments with Cheetah-cub, a compliant quadruped robot. *Int. J. Robot. Res.* **2013**, *32*, 932–950.
42. Chen, S.; Zhang, B.; Mueller, M.W.; Rai, A.; Sreenath, K. Learning Torque Control for Quadrupedal Locomotion. *arXiv* **2023**, arXiv:cs.RO/2203.05194.
43. Agrawal, A.; Chen, S.; Rai, A.; Sreenath, K. Vision-Aided Dynamic Quadrupedal Locomotion on Discrete Terrain Using Motion Libraries. In Proceedings of the 2022 International Conference on Robotics and Automation (ICRA), Philadelphia, PA, USA, 23–27 May 2022; pp. 4708–4714. [[CrossRef](#)]
44. Meng, X.; Wang, S.; Cao, Z.; Zhang, L. A review of quadruped robots and environment perception. In Proceedings of the 2016 35th Chinese Control Conference (CCC), Chengdu, China, 27–29 July 2016; pp. 6350–6356. [[CrossRef](#)]
45. Zha, F.; Chen, C.; Guo, W.; Zheng, P.; Shi, J. A free gait controller designed for a heavy load hexapod robot. *Adv. Mech. Eng.* **2019**, *11*, 1687814019838369. [[CrossRef](#)]
46. Zenker, S.; Aksoy, E.E.; Goldschmidt, D.; Wörgötter, F.; Manoonpong, P. Visual terrain classification for selecting energy efficient gaits of a hexapod robot. In Proceedings of the 2013 IEEE/ASME International Conference on Advanced Intelligent Mechatronics, Wollongong, Australia, 9–12 July 2013; pp. 577–584. [[CrossRef](#)]

47. Kong, B. Modeling and Algorithm Implementation of Free Gait Planning for Quadruped Robot Based on Machine Vision. In Proceedings of the 2021 International Conference on Networking, Communications and Information Technology (NetCIT), Manchester, UK, 26–27 December 2021; pp. 196–199. [[CrossRef](#)]
48. Gong, Z.; Zhang, Y.; Lu, D.; Wu, T. Vision-Based Quadruped Pose Estimation and Gait Parameter Extraction Method. *Electronics* **2022**, *11*, 3702. [[CrossRef](#)]
49. Chen, Z.; Li, J.; Wang, J.; Wang, S.; Zhao, J.; Li, J. Towards hybrid gait obstacle avoidance for a six wheel-legged robot with payload transportation. *J. Intell. Robot. Syst.* **2021**, *102*, 60. [[CrossRef](#)]
50. Zhang, S.; Liu, M.; Yin, Y.; Rong, X.; Li, Y.; Hua, Z. Static Gait Planning Method for Quadruped Robot Walking on Unknown Rough Terrain. *IEEE Access* **2019**, *7*, 177651–177660. [[CrossRef](#)]
51. Wang, J.; Lewis, M.; Gennari, J. Interactive simulation of the NIST USAR arenas. In Proceedings of the SMC'03 Conference Proceedings, 2003 IEEE International Conference on Systems, Man and Cybernetics. Conference Theme—System Security and Assurance (Cat. No.03CH37483), Washington, DC, USA, 8 October 2003; Volume 2, pp. 1327–1332. [[CrossRef](#)]
52. Lambert. Papers with Code—MSEG Dataset. 2021. Available online: <https://paperswithcode.com/dataset/mseg> (accessed on 1 June 2023).
53. Mortimer. Papers with Code—TAS-nir Dataset. 2022. Available online: <https://paperswithcode.com/dataset/tas-nir> (accessed on 1 June 2023).
54. Metzger. Papers with Code—tas500 Dataset. 2021. Available online: <https://paperswithcode.com/dataset/tas500> (accessed on 1 June 2023).
55. Fortin. Papers with Code—timberseg 1.0 Dataset. 2022. Available online: <https://paperswithcode.com/dataset/timberseg-1-0> (accessed on 1 June 2023).
56. Jiang. Papers with Code—rellis-3d Dataset. 2021. Available online: <https://paperswithcode.com/dataset/rellis-3d> (accessed on 1 June 2023).
57. Filitchkin, P.; Byl, K. Feature-based terrain classification for LittleDog. In Proceedings of the 2012 IEEE/RSJ International Conference on Intelligent Robots and Systems, Vilamoura-Algarve, Portugal, 7–12 October 2012; pp. 1387–1392. [[CrossRef](#)]
58. Haddeler, G.; Yee, M.; You, Y.; Chan, J.; Adiwahono, A.H.; Yau, W.Y.; Chew, C.M. Traversability analysis with vision and terrain probing for safe legged robot navigation. *arXiv* **2022**, arXiv:2209.00334.
59. Wermelinger, M.; Fankhauser, P.; Diethelm, R.; Krüsi, P.; Siegwart, R.; Hutter, M. Navigation planning for legged robots in challenging terrain. In Proceedings of the 2016 IEEE/RSJ International Conference on Intelligent Robots and Systems (IROS), Daejeon, Republic of Korea, 9–14 October 2016; pp. 1184–1189. [[CrossRef](#)]

Disclaimer/Publisher's Note: The statements, opinions and data contained in all publications are solely those of the individual author(s) and contributor(s) and not of MDPI and/or the editor(s). MDPI and/or the editor(s) disclaim responsibility for any injury to people or property resulting from any ideas, methods, instructions or products referred to in the content.